

# Robust Person Re-identification with Multi-Modal Joint Defence

Yunpeng Gong  
fmonkey625@gmail.com

Lifei Chen  
clfei@fjnu.edu.cn

## Abstract

The Person Re-identification (ReID) system based on metric learning has been proved to inherit the vulnerability of deep neural networks (DNNs), which are easy to be fooled by adversarial metric attacks. Existing work mainly relies on adversarial training for metric defense, and more methods have not been fully studied. By exploring the impact of attacks on the underlying features, we propose targeted methods for metric attacks and defence methods. In terms of metric attack, we use the local color deviation to construct the intra-class variation of the input to attack color features. In terms of metric defenses, we propose a joint defense method which includes two parts of proactive defense and passive defense. Proactive defense helps to enhance the robustness of the model to color variations and the learning of structure relations across multiple modalities by constructing different inputs from multimodal images, and passive defense exploits the invariance of structural features in a changing pixel space by circuitous scaling to preserve structural features while eliminating some of the adversarial noise. Extensive experiments demonstrate that the proposed joint defense compared with the existing adversarial metric defense methods which not only against multiple attacks at the same time but also has not significantly reduced the generalization capacity of the model. The code is available at [https://github.com/finger-monkey/multi-modal\\_joint\\_defence](https://github.com/finger-monkey/multi-modal_joint_defence)

## 1. Introduction

In general, Person Re-identification (ReID) is viewed as a retrieval task, which ranks a gallery of images by order of similarity to a query image. Therefore, the ReID is usually regarded as a metric learning problem. This is an open-set task where identities at training do not overlap with those at testing. The ReID model uses a metric function to measure the pairwise distances between the query image and gallery images [1], making adversarial metric attacks very different from adversarial classification attacks [2–6]. The adversarial metric attack cheats a ReID model by interfer-



Figure 1. Illustration of an adversarial attack by distorting the color domain, where (a) and (b) show the retrieval results from the clean examples and the adversarial examples under the metric attack from [7], respectively. The numbers on the images indicate the rank of similarity in the retrieval results, and the images with red (green) number correspond to the wrong (correct) results.

ing with the image to modify the distance between image features, which means that it needs a reference image to alter the distance between the attacked image and other images with the same identity. Existing work of [7–10] has fully proved that the ReID models are susceptible to metric attacks from adversarial examples. Since the adversarial defense of ReID has not been fully studied, it remains a challenging problem to effectively defend while ensuring the generalization capability of the model. In our study, we observed that the intra-class variations caused by color deviations such as lighting, chromatic aberration, resolution, etc. in the variable camera conditions have brought potential challenges to the adversarial robustness of model. Due to the training set solely encompasses a limited portion of the intra-class variations of the color domain, a potential target of the adversarial attack is to distort the color domain of the clean example with a slight noise, causing the normally trained model to make mistakes in color. As shown in Figure 1, the perturbation of the adversarial attack alters the color features of the examples, making the model misjudge the color of the pedestrian dress. Based on the above observations, the targeted use of color features to strengthen the attack can be considered. We use local color deviation to construct the intra-class variation of the input to strengthen the attack on color features. Considering that being bet-

ter at capturing shape or contour features is the main factor for the robustness of adversarial training [11] and enhancing the robustness against color variations may be helpful to defense, we seek to construct the diversity of data through sketch-modal images with contour features and grayscale-modal images with color irrelevance to enforce the network learns shape or contour features from the common structure relationship across multi-modal images, and enhances the robustness against color variations. Then we use more image transformation to increase the diversity of the data, so as to further enhance the robustness of the model as a proactive defense of the model. In addition, we use the structural invariance in the process of image scaling to preserve the structural information and damage the adversarial noise as a passive defense of the model to achieve complementarity with proactive defense.

As far as we know, adversarial training is the only adversarial metric defense method that has been proposed. For adversarial training, a defense model trained by adversarial examples of an attack cannot defend against multiple attacks at the same time, and extreme overfitting during training leads to obvious reduction in model generalization capacity. In our joint defense paradigm, not only get rid of the dependence on adversarial training but also overcome the above shortcomings. Our joint defense has the following advantages:

It is a lightweight approach that does not require any additional parameter learning and can be combined with various ReID models without changing the learning strategy. It improves the robustness of the model and performs well in cross-domain tests, which effectively defend against multiple attacks without reducing the generalization capacity of the model.

The main contributions of this paper are summarized as follows:

- We studied adversarial attacks and defenses from a new perspective of the impact of attacks on underlying features.
- We propose a supplement of adversarial metric attack from the perspective of attack color features.
- We propose a robust multi-modal defence which uses proactive and passive defenses to jointly defend against the multiple adversarial metric attacks.
- An interpretable defense analysis is given, which provides direction for enhancing the robustness and security of the ReID system.

## 2. Related Work

In this section we review the previous work on adversarial attacks and defenses for metric learning problems.

### 2.1. Adversarial Attacks

Generally speaking, adversarial attacks can be categorized into white-box, gray-box, and black-box attacks. The

difference between these attacks lies in the knowledge of the adversaries. Black-box attack means that the attacker does not know the structure and parameters of the target network, and is used to attack another network which differs in structures and parameters. White-box attack assumes that the attacker has prior knowledge of the target networks, including the structure and parameters of model, which means that the adversarial examples are generated with and tested on the same network. Gray-box attack assumes that the attacker knows the structure of the target model, that is, the adversarial examples are generated with a network having parameters and used to attack another which differs in parameters. For the same attack, the white-box attack is the strongest compared to the other two.

Metric attacks were first proposed in the security study of ReID to mislead metric task retrieval failures by attacking metric distances. [7] extended some metric attack by classification attacks, including Fast-Gradient Sign Method (FGSM) [2], Iterative FGSM (IFGSM) and Momentum IFGSM (MIFGSM) [5]. Among the three attack methods, IFGSM delivers the strongest white-box attacks. Opposite-Direction Feature Attack (ODFA) [10] exploits feature-level adversarial gradients to generate adversarial examples to pull the feature in the opposite direction with an artificial guide. Self Metric Attack (SMA) [8] uses the image with added noise as the reference image and obtains the adversarial examples by attacking the feature distance between the original image and the reference image. This process does not require any additional images. It is more in line with the actual situation that the attacker usually lacks data. Deep Mis-Ranking (DMR) [9] proposed a learning-to-mis-rank formulation to perturb the ranking of the system output, which used a multi-stage network architecture that pyramids the features of different levels to extract general and transferable features for the adversarial perturbations. Its success attack rate of black-box attacks is almost as high as that of white-box attack. At the same time, it also shows that when applied to classification attacks, it has a higher success attack rate than DeepFool [4], NewtonFool [6], and CW [3].

### 2.2. Adversarial Defenses

Up to now, many effective defense methods have been proposed against adversarial classification attacks, which mainly include denoising methods, randomization-based schemes, adversarial training and so on. In terms of denoising, Guo et al. [12] proposed to adopt more diversified non-differentiable image transformation operations such as depth reduction, total variance minimization and image quilting to increase the difficulty of network gradient prediction to achieve the purpose of defense. Noting that most of the training images are in JPG format, Dziugaite [13] uses JPG image compression method to reduce the impact

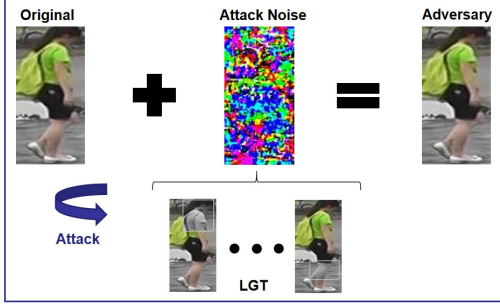


Figure 2. Schematic diagram of Local Transformation Attack. It pushes the feature of the reference image away from the original image by constructing a reference image with local difference from the original image in each basic iteration based on LGT.

of adversarial disturbance. In terms of randomization, RRP (Random Resizing and Padding) [14] mitigates adversarial effects by combining random resizing and random padding based on adversarial training, which achieves a surprising effect against adversarial classification attacks on the ImageNet classification. [15–18] show that adversarial training is a robust way to defend against adversarial attacks, which includes offline adversarial training and online adversarial training.

The metric defense schemes proposed by [7, 8] correspond to offline adversarial training and online adversarial training respectively. The defense method used in [7] is offline adversarial training, which is based on a generation of an adversarial version of the training set obtained with a frozen version of the trained model. As a frozen model is used to generate attacks, this method is referred to as offline adversarial training. The defense method used in [8] is online adversarial training, which generates adversarial examples online while the defended model evolves. However, adversarial training is prone to overfitting because dependent on the training data, so it usually reduces the generalization capacity of the model and still has a high misclassification rate for the adversarial examples from other attacks, which is its main deficiency. Enhancing the robustness towards adversarial examples and maintaining the generalization capacity of the model is the principal problem of adversarial defense.

### 3. Proposed Methods

In this section, we first introduce our design scheme which uses color features to attack and then introduce our multi-modal joint adversarial defense method.

#### 3.1. Local Transformation Attack

To attack against color features, we adopt Local Grayscale Transformation (LGT) [19] constructing the local color deviation of the input, which randomly selects a rectangular area in the image and replaces it with the

pixels of the same rectangular area in the corresponding grayscale image. As shown in Figure 2, the LGT makes the constructed reference image have appropriate local differences from the original image. We call such an attack Local Transformation Attack (LTA). The basic components of ReID metric attack are described in detail in [7], and will not be repeated here.

LTA is defined as the following iterative optimization:

$$x_{adv}^{(0)} = x \quad (1)$$

where  $x$  the attacked image,  $x_{adv}^{(n)}$  the adversarial example at the  $n$ -th iteration.  $\hat{x}^{(n)}$  is the reference image with local variability constructed by LGT at the  $n$ -th basic iteration.

$$\hat{x}^{(n)} = LGT(x) \quad (2)$$

$$x_{adv}^{(n+1)} = \Psi_x^\epsilon(x_{adv}^{(n)} + \alpha \cdot \text{sign}(\text{grad}^{(n+1)})) \quad (3)$$

where  $\epsilon$  the adversarial bound and  $\alpha$  the iteration step size,  $\Psi_x^\epsilon$  the clip function, which ensures that  $\|x_{adv}^{(n+1)} - x\|_\infty < \epsilon$  and that adversarial noise inconspicuousness.

$$\text{grad}^{(n+1)} = \theta \cdot \text{grad}^{(n)} + \frac{\Delta_{LTA}^{(n)}}{\|\Delta_{LTA}^{(n)}\|_1} \quad (4)$$

where  $\text{grad}^{(n)}$  is the accumulated gradient at the  $n$ -th iteration,  $\theta$  the decay factor of the momentum term which is set to 1 in the experiments of this paper.

$$\Delta_{LTA}^{(n)} = \frac{\partial D(x_{adv}^{(n)}, \hat{x}^{(n)})}{\partial x_{adv}^{(n)}} \quad (5)$$

$$D(x_{adv}^{(n)}, \hat{x}^{(n)}) = \|x_{adv}^{(n)} - \hat{x}^{(n)}\|_2^2 \quad (6)$$

Specifically, each basic iteration optimizes adversarial noise by attacking the feature distance between the adversarial image generated from the previous basic iteration and the new reference image.

#### 3.2. Proposed Adversarial Defence

In this subsection, we introduce the *multi-modal joint adversarial defense* (JAD) proposed in this paper, which includes the proactive defense composed by *channel fusion* (CF) and *diversity learning* (DL) as well as the passive defense composed by *circuitous scaling* (CS). Finally, we clarify the limitations of DL.

**Channel Fusion.** A grayscale image is a visible image that loses some color information, and a sketch image is a grayscale image that loses some detailed information. Thus, visible images, grayscale images, and sketch images are homogeneous which contain the same structural information. [19, 20] show that the use of homogeneous images in training to learn structural information positively contributes to the performance of the model. The shape and

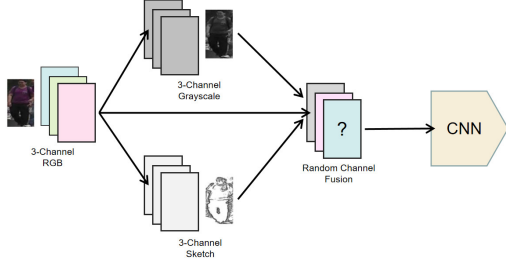


Figure 3. Schematic diagram of multi-modal images channel fusion.



Figure 4. Example diagram of channel fusion.

contour features emphasized by adversarial training are all included in the structural information of the image. By adding multi-modal images with the same structure information to the training data, the proposed method helps the model strengthen learning the structure features of the data.

CF combines the three modal images of visible (RGB), grayscale and sketch for random channel fusion. We adopt the default operation Grayscale(3) in Pytorch to get the grayscale image for each visible image, and sketch images can be obtained by inverting the grayscale image and then Gaussian blurring it, finally blending it with the grayscale image. As shown in Figure 3, the RGB images are randomly converted with a certain probability into 3-channel grayscale images or sketch images in pre-processing stage, and then randomly merge the channels of the grayscale image and the sketch image with the channels of the RGB image to create a new homogeneous modal image. The advantages of using homogeneous modal images can be attributed to two aspects: (1) the homogeneous images retain the information structure of visible images, which ensures the model converges normally. (2) It brings rich variation to the input images simply and effectively.

In the experimental setting, the image is converted into a grayscale image with a probability of 5% directly input to the deep convolutional neural network (CNN). In addition, the image is converted into a grayscale image with a probability of 1% and sketch image with a probability of 1% for CF. In the process of CF, 1 or 2 channels are randomly selected from the R, G, and B channels of the visible image. After the selected visible image channel and the number of channels  $N$  are determined, the grayscale or sketch image channel is randomly selected to reconstruction a new

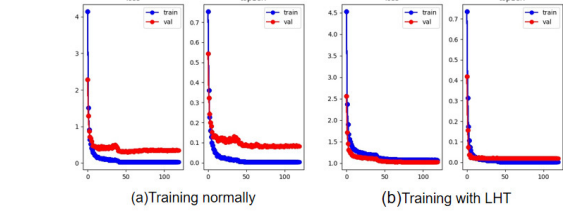


Figure 5. The comparison of training curve.

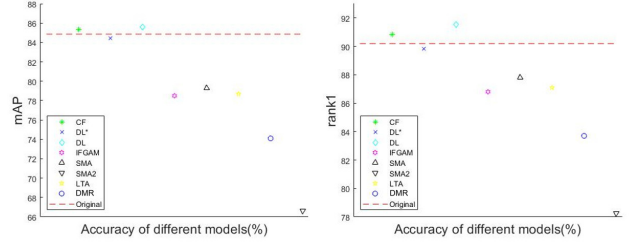


Figure 6. Comparison of accuracy of defense model on the Market-1501 dataset.

3-channel image. In fact, a maximum of 60 homogeneous variations can be generated by combining the 5 image channels types of R, G, B, grayscale, and sketch in random order.

**Diversity Learning.** Image transformation such as Posterize, Equalize, Solarize, Contrast, Inversion, etc. are adapted to further extend the diversity of image modalities based on CF. However, too many input variations will lead to overfitting of the model, which affects the generalization capacity of the model as shown in Figure 5(a). To solve this problem, we extend LGT to *local homogeneous transformation* (LHT) to help the model to fit the diversity of variation gradually from local variations. The difference with LGT is that LHT replaces randomly selected regions with homogeneous images. As shown in Figure 5(b), it positively helps reduce the overfitting in training. Unless otherwise specified, the diversity learning in subsequent experiments combine with LHT by default.

The advantages of the our method on Market1501 [21] compared to the adversarial training in the generalization capacity are shown in Figure 6. CF, DL\* and DL in the figure are the defense models proposed in this paper, and IFGSM [7], SMA [8], LTA, and DMR [9] are the offline adversarial training defense models corresponding to the attacks. It can be seen that the accuracy of the offline adversarial training model is significantly lower than that of the normally trained model. Where SMA2 is the online adversarial training model of SMA attack, and its accuracy is the lowest. In practice, we found that the online adversarial training of some attacks is even difficult to converge, so in the following experiments we only compare offline adversarial training.



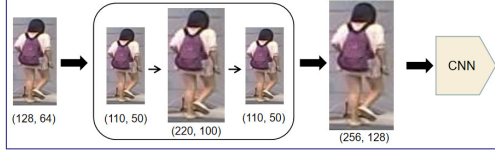


Figure 7. Schematic diagram of CS.

**Circuitous Scaling.** The part of passive defense is realized by a series of image resizing. Taking the Market1501 dataset as an example, the original size of the dataset image is  $[128, 64]$ , and the size is uniformly resized to  $[256, 128]$  when fed into the CNN. When using image resizing as passive defense, we observed that the network performance hardly drops and gets a satisfactory defense effect if we resize the image to  $[110, 50]$  to corrupt the adversarial noise structure. Our passive defense composed by a series of resizing that resize the image to  $[110, 50]$  then to  $[220, 100]$ , then to  $[110, 50]$  again (finally uniformly to the  $[256, 128]$ ), so it called *circuitous scaling*. The effect of image scaling (only once resizing) and CS on the adversarial noise can be seen in Figure 8, and it can be observed that the adversarial noise at the contour features is continuously weakened, and the outline of the pedestrian is more clearer.

**Limitations of DL.** In the study, we observed that the models trained by DL did not always enhance the adversarial robustness of the models. For example, we trained 8 models independently, and 4 of them did not enhance, while the other 4 models got some degree of adversarial robustness, with 1 got the best defense. We speculate that when the neural network is optimized, it does not always toward the direction of robustness, and sometimes toward overfitting (in other senses). Fortunately, we observed that the adversarial robustness of the model is consistent with the performance of cross-domain tests. Therefore, a possible solution is to use cross-domain tests to determine whether to update the model parameters during the model training as a way to ensure that the trained model enhances the adversarial robustness.

## 4. Experiments

In this section, We evaluate the attack against color features by comparing with SMA and then evaluated the robustness of our approach using cross-domain tests. Finally, we verify the effectiveness of our JAD through extensive experiments.

### 4.1. Attack Evaluation and Cross-Domain Tests

**Datasets.** We conducted experiments on Market1501 and DukeMTMC. The Market1501 [21] includes 1,501 pedestrians captured by six cameras (five HD cameras and one low-definition camera). The DukeMTMC [22] is a

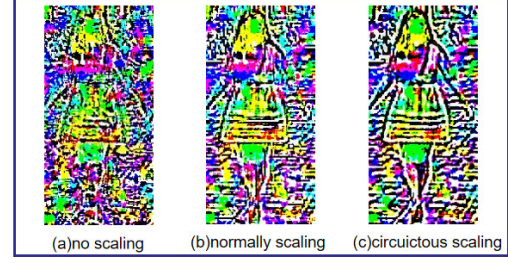


Figure 8. The effect of image scaling and CS on the adversarial noise, where (a) shows the adversarial noise from the original adversarial example, and (b) shows the adversarial noise after resize the adversarial sample to  $[110, 50]$  (then restored to  $[256, 128]$ ). (c) shows the adversarial noise after CS.

large-scale multi-target, multi-camera tracking dataset, a HD video dataset recorded by 8 synchronous cameras, with more than 2,700 individual pedestrians. The above two datasets are widely used in ReID studies.

**Evaluation criteria.** Following existing works, Rank-k precision and mean Average Precision (mAP) are adapted as the evaluation metrics. Rank-1 denotes the average accuracy of the first returned result corresponding to each query image. mAP denotes the mean of average accuracy, the query results are sorted according to the similarity, the closer the correct result is to the top of the list, the higher the score.

**Implementation Details.** The proposed adversarial attack and defense algorithm is development based on [23]. ResNet50 [24] and DenseNet [25] are used as the backbone network in experiments, and the pre-trained ImageNet parameters are adopted for network initialization. Specifically, the stride of the last convolutional block is set to 2. We adopt the stochastic gradient descent (SGD) optimizer for optimization, and the momentum parameter is set to 0.9. We set the initial learning rate as 0.1. The learning rate is decayed by 0.1 every 40 iteration, with a total of 60 training epochs and a batch size of 32 for normal training on both datasets, and 120 training epochs for the proposed method used in this paper as well as for adversarial training.

**Attack Evaluation.** The hyper-parameters are unified for fair comparison, the adversarial boundary is set to 5 pixels, the iteration step size is set to 1, and the number of basic iterations is set to 15. Note that in contrast to an adversarial defense problem, lower precision indicates better attack performance. It can be seen from Table 1 that when only one version of the reference image is used, the success attack rate of LTA- is better than that of SMA. The comparison between LTA- and LTA shows that using diverse versions of reference images has a higher attack success rate than using only one version of reference images. The experimental results fully demonstrate that the attack against

Table 1. Evaluation on Market1501 under a white-box attack on the query set. Where LTA- means that only one version with local differences is used as a reference image, and LTA generates image versions with different local differences in each basic iteration to conduct the metric attack.

Attack	Rank1	Rank5	Rank10	mAP
Original	88.4%	95.5%	97.1%	72.1%
SMA	15.7%	26.4%	32.7%	11.1%
LTA-(ours)	15.7%	26.2%	32.1%	11.0%
LTA(ours)	13.3%	22.4%	28.1%	9.6%

color features are more aggressive compared to the same type of SMA attack.

**Cross-Domain Tests.** It is pointed out by [7] that the higher accuracy of the model does not mean that it has better generalization capacity. The defense capabilities of different baselines under the same attack would have been greatly different, and the high accuracy model may even have worse defenses capabilities due to overfit. In response to the above potential problems, we use cross-domain tests and adversarial defense tests to verify the robustness of the model. Experiments show that the proposed method effectively enhances the generalization capacity of the model, and the Table 2 shows the cross-domain experiments of the proposed method between two datasets, Market-1501 and DukeMTMC. To be consistent with recent works, we follow the new training/testing protocol to conduct our experiments by k-reciprocal re-ranking [26]. If we do not specify, the subsequent experimental results were tested with re-ranking.

In the cross-domain tests of  $M \rightarrow D$ , it can be seen that the  $DL^*$  (diversity learning without using LHT) enhances the Rank1 by 3.1 percentage points compared with the normally trained model, and further enhances by 4.8 percentage points after using LHT. In the cross-domain tests of  $D \rightarrow M$ , it can be seen that the  $DL^*$  enhances the Rank1 by 3.4 percentage points compared with the normal training model, and further enhances by 0.2 percentage points after using LHT. The above shows that diversity learning effectively enhances the generalization capacity of the model, and LHT further enhances the generalization capacity, which means that diversity learning and LHT both enhance the robustness of the model.

## 4.2. Experiments of JAD

This subsection verifies the effectiveness of the proposed method from white-box attack, black-box attack and the other baselines, and shows the effect of each component of the proposed method in defense through ablation experiment. Then, the proposed method is compared with adversarial training (AT) and RRP. Finally, we give a visual

Table 2. The performance of different models is evaluated on cross-domain dataset.  $M \rightarrow D$  means that we train the model on Market1501 and evaluate it on DukeMTMC. RK stands for the results obtained by re-ranking.

Model	$M \rightarrow D$		$D \rightarrow M$	
	Rank-1	mAP	Rank-1	mAP
Normal	36.1%	18.9%	45.7%	19.6%
Normal+RK	41.4%	30.1%	49.5%	28.8%
$DL^*$	36.9%	18.4%	47.4%	19.5%
$DL^*+RK$	44.5%	31.4%	52.9%	30.9%
$DL^*+LHT$	42.5%	21.5%	47.5%	19.4%
$DL^*+LHT+RK$	49.3%	36.6%	53.1%	30.3%

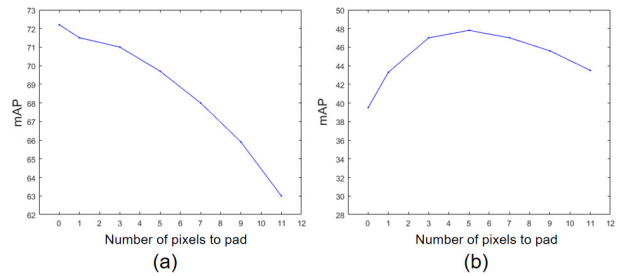


Figure 9. (a) shows the effect of padding on the performance of the original model and (b) shows the effect of padding on the performance of defence

analysis of our defense.

AT is the defense method currently used for adversarial metric defenses. For a fair comparison, we extend it to RRP, which is composed by combining random operations of the resizing and padding based on AT. In order to quantitatively analyze and compare fairly, we fix the image scaling parameters to [110, 50] and explore the optimal parameters for the padding layer under SMA white-box attack on Market1501. As shown in Figure 9, it is observed that the model generalization capacity decreases as the number of filled pixels increases, and the best defense accuracy is achieved at the number of filled pixels of 5. Therefore, we conduct comparison experiments with the parameters that RRP achieve the best defense accuracy, i.e.  $resize(110,50)$  and  $pad(5)$ .

We tested the JAD with white-box attacks on Market1501 and DukeMTMC, and the attacks include IFCSM, SMA and LTA. Where  $N$  means that the model is obtained by normal training without any defense.

It can be seen from Table 4 that on the two datasets, our JAD has enhanced the Rank-1 in all white-box attacks by more than 40 percentage points after using re-ranking.

**Ablation studies.** We studied the contributions of our CF, DL and JAD. From Table 5, we can see that defense accuracy increases with the increase of data diversity. As a passive defense in our JAD, CS further significantly enhances defense performance. Table 6 shows that CS effectively reduces the adversarial effect and thus significantly

Table 3. Performance of normally trained models and our JAD models on Market1501 and DukeMTMC.

Methods	Market1501(M)		DukeMTMC(D)	
	Rank1	mAP	Rank1	mAP
Normal	88.4%	72.2%	78.7%	62.3%
Normal+RK	90.2%	84.7%	83.3%	79.3%
JAD	88.7%	70.3%	77.2%	57.8%
JAD+RK	91.0%	85.0%	82.7%	77.0%

Table 4. Performance of normally trained models and our JAD models under white-box attack of the query.

Dataset	Model	Rank-1/mAP(%)		
		IFGSM	SMA	LTA
M	N	8.1/4.3	15.7/11.1	13.3/9.6
	N+RK	13.2/13.0	17.6/20.0	14.2/16.1
	JAD	47.1/27.8	79.3/60.1	56.5/41.1
	JAD+RK	61.3/56.8	85.6/80.3	66.2/63.9
D	N	10.1/5.8	15.0/10.4	13.0/9.2
	N+RK	16.8/16.3	18.8/19.8	15.2/16.3
	JAD	30.5/16.3	56.7/39.5	41.8/27.6
	JAD+RK	48.1/43.4	69.3/64.5	52.4/49.7

Table 5. Comparison the defense accuracy of normally trained models, channel fusion, diversity learning, and joint adversarial defense under white-box attack on Market1501.

Model	Rank-1/mAP(%)			
	Original	IFGSM	SMA	LTA
N	90.2/84.7	13.2/13.0	17.6/20.0	14.2/16.1
CF	90.8/85.3	18.3/16.7	18.0/19.6	17.1/18.5
DL	91.5/85.6	31.7/28.7	58.4/57.1	25.2/27.6
JAD	91.0/85.0	61.3/56.8	85.6/80.3	66.2/63.9

enhances the defense with negligible performance degradation.

**Comparison of State-of-the-Arts.** AT needs to be customized according to attacks. Specifically, in order to defend an attack, it is necessary to add corresponding adversarial examples to train the model. In Table 7, the original accuracy (test on clean images) of defense methods based on AT are the average accuracy of the defense models corresponding to the three attacks. Where AT\_CS is the defense model combining the AT and our CS, and it can be seen that the DL and CS (that is, our JAD) exert a better combined effect. We infer that the overfitting of the model to the adversarial examples leads to lack of generalization capacity to the denoised adversarial examples thus inhibits the combined effect. The defense performance of our JAD is close to RRP and may exceed it. To verify this, we resize the image to [90, 40] then to [200, 90], then to [90, 40]

Table 6. Comparison the defense accuracy of different resizing combinations. Where A means resize image to [110, 50] and B means resize to [220, 100]. AB means resize image to [110, 50] then to [220, 100]. N means the normally trained model. Original means the test result on clean images.

Dateset	Model	Original	LTA Attack
		Rank-1/mAP(%)	Rank-1/mAP(%)
M	N	90.2/84.7	14.2/16.1
	N+A	90.0/84.7	25.5/27.5
	N+B	90.3/84.9	15.9/17.9
	N+AB	90.1/84.8	25.8/27.8
	N+ABA	89.8/84.3	<b>31.4/33.1</b>

Table 7. Comparison the defense accuracy of different defense methods under white-box attacks on Market1501.

Model	Rank-1/mAP(%)			
	Original	IFGSM	SMA	LTA
N	90.2/84.7	13.2/13.0	17.6/20.0	14.2/16.1
AT	86.4/76.9	46.8/41.3	48.3/47.4	49.1/48.4
AT_CS	86.4/78.1	60.6/53.8	64.9/61.1	62.7/58.5
RRP	85.0/75.3	67.5/58.3	74.0/66.8	70.9/64.4
JAD	91.0/85.0	61.3/56.8	85.6/80.3	66.2/63.9
JAD2	90.6/84.3	66.9/62.1	<b>86.5/80.7</b>	73.5/69.5
JAD3	86.8/78.5	<b>71.9/63.7</b>	83.8/75.4	<b>76.3/69.0</b>

Table 8. Comparison the defense accuracy of different defense methods and other baselines under DMR black-box attack.

Model	Rank-1/mAP(%)		Model	Rank-1/mAP(%)	
	Original	DMR		Original	DMR
N	92.1/86.7	25.2/27.1	SB	95.4/94.2	6.2/4.8
AT	91.1/85.8	88.7/83.5	SB+JAD	95.1/94.0	93.3/91.2
RRP	89.4/83.3	85.0/79.1	FR	96.8/95.3	24.8/25.9
JAD	92.4/87.5	<b>89.6/84.1</b>	FR+JAD	96.3/94.9	<b>91.6/90.1</b>

again to obtain the JAD2 model. As with RRP, even if the attacker is aware of the existence of passive defenses, CS can still be effectively defended by a randomization mechanism that allows the resize to fluctuate within a certain range. It can be seen that the defense performance of our JAD2 model beats RRP, which hardly drops original performance. Where JAD3 adds pad(5) operation on the basis of our JAD. It can be seen that its defense performance is far more than RRP. Compared with AT, our JAD3 enhances Rank1 by more than 24% in all white-box attacks.

In the tests of DMR black-box attack, we used adversarial examples generated by Resnet50 to attack the DenseNet model. It can be seen from Table 8 that the defense accuracy of our JAD is better than AT, while RRP is at a disadvantage in terms of defense performance may be due to higher negative impact on the generalization capacity. In addition, the experimental results show that the JAD is ap-

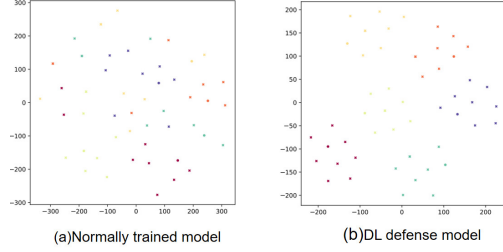


Figure 10. t-SNE [30] visualization of six randomly selected images with different identities on Market1501. Each image corresponds to an IFGSM adversarial example and some randomly generated homogeneous modalities images. The same color means that they are obtained by transformation of the same image. Dots means adversarial example.

Table 9. Comparison the success attack rate of adversarial examples generated by normally trained model and DL model under gray-box attack.

Attack source	Rank1	Rank5	Rank10	mAP
Normal model	61.0%	78.4%	84.3%	45.9%
DL model	84.3%	93.2%	95.3%	66.6%

plicable to other baselines and performs well. Where Strong Baseline (SB) [27] is implemented based on the Resnet50 backbone network adding the Batch Normalization Neck structure, and FastReID (FR) [28] is implemented based on the IBN-ResNet101 [29] backbone network. All in all, the method proposed in this paper has good defense effect in both white-box attack and black-box attack.

**Visualization Analysis.** As the show in Figure 10, the multi-modal defense model with structural invariance which is insensitive to the variations in the adversarial examples relative to the original examples. Therefore, we can observe that the features of adversarial example and homogeneous examples exhibit clustering effects.

We use SMA to conduct white-box attacks on the normally trained model and our DL model respectively. It can be observed that the adversarial noise in Figure 11(d) is sparser than Figure 11(b), which indicates that the attacker shows less aggressive to the DL defense model and implies that DL effectively enhances the robustness of the model.

A gray-box attack is conducted on normally trained model using the adversarial examples of another normally trained model and DL models. The experimental results in Table 9 show that the adversarial examples generated on the DL model are less aggressive than generated on the normally trained model. It shows that a model with adversarial robustness increases the difficulty of an attacker to implement attacks.

Grad-CAM [31] uses the gradient information flowing into the last convolutional layer of the CNN to visualize the importance of each neuron in the output layer for the final

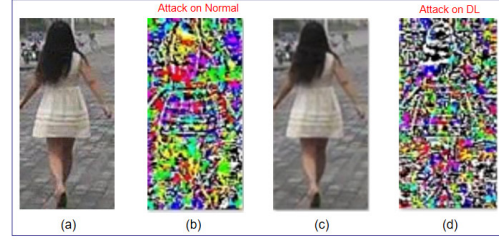


Figure 11. (a) and (c) shows the adversarial example of the normally trained model and DL model under SMA white-box attack, and (b) shows the adversarial noise of (a). (d) shows the adversarial noise of (c).

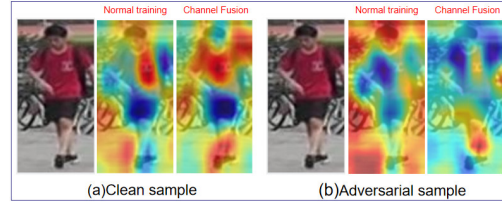


Figure 12. Comparison of Grad-CAM activation map between normally trained model and CF model. (a) shows the activation maps of clean example on the normally trained model and CF defense model, and (b) shows the activation maps of adversarial example on the normally trained model and CF defense model.

prediction, by which it is possible to visualize which regions of the image have a significant impact on the prediction of a model. As shown in Figure 12(b), we can see that the adversarial example successfully distracts the attention of the normally trained model and activates the opposite parts, while the our CF defense model is still effectively activating some important parts.

This section draws the following conclusions from the visual analysis. By learning diverse modalities data, the defense model with structural invariance which is insensitive to the variations in the adversarial examples relative to the original examples. The robustness of model makes the adversarial noise sparse, which means less misleading to model, so the model can still activate regions critical to prediction when attacked by adversarial samples.

## 5. Conclusion

In this paper, we gained insight into the impact of attacks on underlying features, and propose a homogeneous diversification-based mechanism to enhance the adversarial robustness of ReID. On the one hand, we conduct comprehensive experiments to validate the effectiveness of the proposed defense method, using different network structures and baselines under different attack methods. The experimental results show that with the increase of diverse modalities, the adversarial robustness of the model also increases, and gradually learning diversity data from local variations helps the network fit better. On the other hand, we analyze the adversarial robustness of the proposed defense method



using visual analysis. Finally, we hope that this study will contribute to the development of deep learning in adversarial defense and inspire future researchers.

## References

- [1] Qingming Leng, Mang Ye, and Qi Tian. A survey of open-world person re-identification. *IEEE TCSVT*, 30(4):1092–1108, 2019. 1
- [2] Ian J. Goodfellow, Jonathon Shlens, and Christian Szegedy. Explaining and harnessing adversarial examples. In *ICLR*, 2014. 1, 2
- [3] Nicholas Carlini and David Wagner. Towards evaluating the robustness of neural networks. *IEEE Symposium on Security and Privacy*, pages 39–57, 2017. 1, 2
- [4] Seyed-Mohsen Moosavi-Dezfooli, Alhussein Fawzi, and Pascal Frossard. Deepfool: a simple and accurate method to fool deep neural networks. In *CVPR*, 2016. 1, 2
- [5] Yinpeng Dong, Fangzhou Liao, Tianyu Pang, Hang Su, Jun Zhu, Xiaolin Hu, and Jianguo Li. Boosting adversarial attacks with momentum. In *CVPR*, 2018. 1, 2
- [6] Uyeong Jang, Xi Wu, and Somesh Jha. Objective metrics and gradient descent algorithms for adversarial examples in machine learning. In *Proceedings of the 33rd Annual Computer Security Applications Conference*, pages 262–277, 2017. 1, 2
- [7] Song Bai, Yingwei Li, Yuyin Zhou, Qizhu Li, and Philip H.S. Torr. Metric attack and defense for person re-identification. arXiv:1901.10650, 2019. 1, 2, 3, 4, 6
- [8] Quentin Bouniot, Romaric Audigier, and Angelique Loesch. Vulnerability of person re-identification models to metric adversarial attacks. In *CVPRW*, 2020. 1, 2, 3, 4
- [9] Hongjun Wang, Guangrun Wang, Ya Li, Dongyu Zhang, and Liang Lin. Transferable, controllable, and inconspicuous adversarial attacks on person re-identification with deep mis-ranking. In *CVPR*, 2020. 1, 2, 4
- [10] Zhedong Zheng, Liang Zheng, Zhilan Hu, and Yi Yang. Open set adversarial examples. arXiv:1809.02681v1, 2018. 1, 2
- [11] Tianyuan Zhang and Zhanxing Zhu. Interpreting adversarially trained convolutional neural networks. In *Proceedings of the 36th International Conference on Machine Learning*, volume 97, pages 7502–7511, 2019. 2
- [12] Chuan Guo, Mayank Rana, Moustapha Cisse, and Laurens van der Maaten. Countering adversarial images using input transformations. In *ICLR*, 2018. 2
- [13] Gintare Karolina Dziugaite, Zoubin Ghahramani, and Daniel M. Roy. A study of the effect of jpg compression on adversarial images. arXiv preprint arXiv:1608.00853, 2016. 2
- [14] Cihang Xie, Jianyu Wang, Zhishuai Zhang, Zhou Ren, and Alan Yuille. Mitigating adversarial effects through randomization. In *ICLR*, 2018. 3
- [15] Aleksander Madry, Aleksandar Makelov, Ludwig Schmidt, Dimitris Tsipras, and Adrian Vladu. Towards deep learning models resistant to adversarial attacks. arXiv:1706.06083, 2017. 3
- [16] Cihang Xie, Yuxin Wu, Laurens van der Maaten, Alan L. Yuille, and Kaiming He. Feature denoising for improving adversarial robustness. In *CVPR*, pages 501–509, 2019. 3
- [17] Nicholas Carlini, Guy Katz, Clark Barrett, and David L. Dill. Ground-truth adversarial examples. In *ICLR*, 2018. 3
- [18] Papernot N, Faghri F, Carlini N, Goodfellow I, Feinman R, Kurakin A, and et al. Technical report on the cleverhans v2.1.0 adversarial examples library. arXiv:1610.00768v6, 2016. 3
- [19] Yunpeng Gong. A general multi-modal data learning method for person re-identification. arXiv:2101.08533v4, 2021. 3
- [20] Mang Ye, Jianbing Shen, Senior Member, IEEE, and Ling Shao. Visible-infrared person re-identification via homogeneous augmented tri-modal learning. *IEEE Transactions on Information Forensics and Security*, 16:728–739, 2021. 3
- [21] Liang Zheng, Liyue Shen, Lu Tian, Shengjin Wang, Jingdong Wang, , and Qi Tian. Scalable person re-identification: a benchmark. In *ICCV*, 2015. 4, 5
- [22] Zhedong Zheng, Liang Zheng, and Yi Yang. Unlabeled samples generated by gan improve the person re-identification baseline in vitro. In *ICCV*, 2017. 5
- [23] Zhedong Zheng, Liang Zheng, and Yi Yang. A discriminatively learned cnn embedding for person reidentification. *IEEE Transactions on Information Forensics and Security*, 16:728–739, 2021. 5
- [24] Kaiming He, Xiangyu Zhang, Shaoqing Ren, and Jian Sun. Deep residual learning for image recognition. In *CVPR*, 2016. 5
- [25] Gao Huang, Zhuang Liu, Laurens van der Maaten, and Kilian Q. Weinberger. Densely connected convolutional networks. In *CVPR*, 2017. 5
- [26] Zhun Zhong, Liang Zheng, Donglin Cao, and Shaozi Li. Re-ranking person re-identification with k-reciprocal encoding. In *CVPR*, 2017. 6
- [27] Hao Luo, Youzhi Gu, Xingyu Liao, Shenqi Lai, and Wei Jiang. Bag of tricks and a strong baseline for deep person re-identification. In *CVPRW*, 2019. 8
- [28] Lingxiao He, Xingyu Liao, Wu Liu, Xinchun Liu, Peng Cheng, and Tao Mei. Fastreid: a pytorch toolbox for general instance re-identification. arXiv:2006.02631, 2020. 8
- [29] Xingang Pan, Ping Luo, Jianping Shi, and Xiaoou Tang. Two at once: enhancing learning and generalization capacities via ibn-net. In *ECCV*, 2018. 8
- [30] L Maaten and G Hinton. Visualizing data using t-sne. *Journal of Machine Learning Research*, pages 2579–2605, 2008. 8
- [31] Ramprasaath R. Selvaraju, Michael Cogswell, Abhishek Das, Ramakrishna Vedantam, Devi Parikh, and Dhruv Batra. Grad-cam: Visual explanations from deep networks via gradient-based localization. In *ICCV*, pages 618–626, 2017. 8